

Satellite Observations of Atmospheric Gravity Waves

D. L. Wu and J. W. Waters

Jet Propulsion Laboratory, California Institute of Technology

Pasadena, CA 91109

Abstract

The Microwave Limb Sounder (MLS) on the Upper Atmosphere Research Satellite has now produced the first global maps of small-scale gravity wave variances in the middle atmosphere. Observations at 30-80km altitudes show that the variances of 30-100km horizontal scales are strongly correlated with surface topography and stratospheric jetstreams. The normalized variance amplitude grows exponentially with height in the stratosphere, and saturates in the mesosphere as expected from wave breaking and dissipation at these altitudes. The several years of MLS data will provide a climatology of global gravity wave activity needed for modeling atmospheric circulations and mixing processes.

Internal gravity waves (IGWs), due to buoyancy forces in Earth's atmosphere, play a fundamental role in driving global circulations and determining thermal/constituent structures [1]. Although they have only 10- 1000km horizontal wavelengths, IGWS can generate significant momentum and energy fluxes through wave breaking, and affect global-scale flows. However, gravity wave forcings are not yet well quantified because adequate global long-term observations are lacking. This uncertainty poses problems for modeling atmospheric general circulations and constituent mixings, particularly in regions, such as the mesosphere and the polar stratosphere, where IGW forcings are relatively strong. Measuring 10-1 000km scale atmospheric variations at 20-80km altitudes has been a great challenge to modern observational techniques. For ground-based radar techniques [2], this altitude region is either too high or low to have sufficient backscattered signals. Most information on IGWs in this region has been provided by rocket soundings [3] and lidar measurements [4] which are limited to a few geographic locations. Satellite remote-sensing has previously provided global measurements of large-scale waves [5], but not of much smaller scale features because of spatial smearing and sparse sampling.

The study presented here shows that the Upper Atmosphere Research Satellite (UARS) Microwave Limb Sounder (MLS) [6], although not designed for this purpose, has an ability to observe small-scale IGW temperature fluctuations at 30-80km altitudes. We obtain the first global maps of IGW variances at these scales, which provide new information on gravity wave distribution, generation, propagation and interactions with background atmospheric flows. The MLS instrument has been measuring pressure, temperature and constituents since September 1991 by step-scanning the atmosphere in 65 seconds from 90km to the surface, at increments of 5km in the mesosphere and 1-

3km in the stratosphere and troposphere. The O_2 radiances measured by the MLS 63GHz radiometer, which are used to retrieve atmospheric tangent pressure and temperature [7], are all saturated when the instrument views tangent heights below -1 Skin. MLS resolves the atmospheric O_2 emission line into 15 spectral channels, and radiances near line-center (channel 8) saturate at higher altitudes than those near the line-wing (channels 1 and 15) because of stronger line-center absorption. The saturated radiance is a good measure of atmospheric temperature and depends little on the tangent pressure of the observing path. As the satellite moves along, fluctuations in the saturated radiances directly reflect atmospheric temperature variations in the horizontal direction.

Instrument spatial resolution and sampling are key to sensing IGW-scale disturbances. Figure 1 gives the temperature weighting functions for 18km tangent height observations, showing various altitude layers between -30 and 80 km that contribute to the saturated radiances with vertical smearings of -10 to 15 km. Horizontal smearings are ~ 100 - 300 km cross-track due to radiative transfer through the limb path (the MLS observation direction is perpendicular to the orbit velocity), and 20 km along-track due to the antenna field-of-view smearing. Because of the vertical and horizontal smearings, amplitudes of MLS radiance fluctuations will be smaller than the actual atmospheric temperature variations but these are detectable due to low instrument noise (varying from 0.06 K for channels 1 and 15, to 0.5 K for channel 8). The integration time for each measurement is ~ 2 seconds, corresponding to ~ 14 km along-track spatial sampling.

The variance of atmospheric fluctuations is derived from total variance of MLS saturated radiances which is computed using 6 consecutive measurements in the bottom of each scan. These atmospheric fluctuations reveal mainly the variations of -30 - 100 km

horizontal scales, and we adopt the common interpretation of fluctuations at these scales as a manifestation of upwardly propagating gravity waves [8]. A weak linear variation, which accounts for the tangent pressure dependence and large-scale wave modulations, is first removed from the 6 radiance measurements. Subsequently, the total variance of the radiance, σ^2 , can be written as

June to 28 July 1993), centered on yaw days. Figure 2 shows the resulting maps at seven altitudes, and striking features in these maps are large amplitudes associated with (a) the stratospheric polar vortex in the winter hemisphere, and (b) subtropical land masses in the summer hemisphere. These features evolve with height and change remarkably above the stratopause.

Background winds are expected to play a major role in determining the IGW variance amplitudes in the stratosphere and mesosphere. Theoretical studies [10,11] show that a strong background wind is a favored condition for IGWs to propagate vertically because then the large intrinsic phase speed (i.e. difference between horizontal wave phase speed and the background wind) prevents the waves from breaking. During solstice periods, the stratospheric polar winter vortex exhibits a very strong westerly wind near 60° latitude throughout the stratosphere and upper troposphere. The selective filtering effect of this wind jet allows up-stream propagating IGWS to grow more efficiently with height than others, and therefore is likely to cause the variance enhancement inside the jetstream. The subtropical variances in the summer hemispheres also suggest this selective filtering function by background winds, showing larger amplitudes at the latitudes (10°S-30°S in “January” and 10°N-30°N in “July”) where winds are stronger. The distribution of these summer IGW variances is consistent with that of the high-wavenumber momentum flux calculated from the GFDLSKYHI high-resolution general circulation model [11], both showing large magnitudes over Madagascar, Australia, South Pacific and Brazil during January.

The variances in Figure 2 also contain information on IGW sources such as tropospheric convection and surface topography. Tropospheric cumulus convection,

frequently occurring in the summer over tropical and subtropical land masses, is most likely responsible for the large stratospheric variances observed near Madagascar, North Australia and Brazil during “January”, and South Asia, Central America and North Africa during “July”. By coupling with the subtropical jet flows, these convective disturbances may propagate efficiently through the stratosphere and become important localized forcings in the mesosphere.

The zonal asymmetries of the wintertime jet streams in the stratosphere are generally believed due to differences in surface topography and tropospheric forcings between the two hemispheres, and IGWS may provide a considerable contribution to such structures. The MLS observations show a strong correlation between the stratospheric variances and high-latitude surface topography. For example, during “January” in the Northern Hemisphere, a broad spectrum of gravity waves is probably generated by the sources associated with surface topography in Europe and North America, which significantly perturbs the zonal symmetry of the jet stream. During “July” in the Southern Hemisphere, large variances basically follow the Antarctic coastline, and are enhanced equatorward over New Zealand and South America.

The variance growth with height, shown in Figure 3, reveals an important behavior of vertically propagating perturbations. Despite very different amplitudes in the lower stratosphere, these variances show approximately the same growth rate with height throughout the stratosphere, which is consistent with the theoretical exponential growth for non-breaking IGWS and also agrees with previous rocket observations [12]. This variance growth further supports the IGW interpretation of the observed radiance fluctuations. In Figure 3, saturation of the variance growth is observed above 50-60 km. It

1

is not clear what mechanisms cause this, but gravity wave saturation is recognized to generate momentum drag and heat in the atmosphere [13]. In Figure 4, zonal means of the normalized variances show that the saturation occurs lower over the stratospheric jetstreams (50°N-70°N in “January” and 50°S-70°S in “July”) and subtropical land masses (10°S-30°S in “January” and 10°N-30°N in “July”). This suggests that the drag force of the observed IGWS would close stratospheric jets at lower altitudes in these places, as is seen in the climatological mean zonal winds during these periods [14]. Moreover, strong dynamic heating from the IGW saturation in the jetstreams may reverse the temperature lapse rate significantly and create temperature inversion layers in the mesosphere. Recent maps of temperature inversions in the mesosphere [15] show a very similar distribution to that of the IGW variances observed by MLS in the stratosphere.

This new global view of IGWs in the middle atmosphere significantly improves our knowledge of gravity wave generation and propagation, and provides an observational basis for refining IGW parameterization schemes used in atmospheric circulation modeling. Further analyses of MLS radiances are underway and will provide a more complete climatology of global long-term gravity wave activity in the stratosphere and mesosphere.

References

1. R. S. Lindzen, *J. Geophys. Res.*, 86, 9707 (1981); T. Matsuno, *J. Meteorol. Soc. Jpn.*, 60, 215 (1982); J. R. Holton, *J. Atmos. Sci.*, 39, 791 (1982); T. J. Dunkerton, *J. Atmos. Sci.*, 39, 1711 (1982).

2. C. E. Meek and A. H. Mason, *Radio Sci.*, **20**, 1383 (1985); R. A. Vincent and D. C. Fritts, *J. Atmos. Sci.*, **44**, 748 (1987); S. Fukao et al., *J. Geophys. Res.*, **99**, 18,973 (1994).
3. I. Hirota, *J. Atmos. Terr. Phys.*, **46**, 767 (1984); S. Eckermann, I. Hirota, and W. K. Hocking, *Q. J. R Meteorol. Soc.*, **121**, 149 (1994).
4. R. Wilson, M.L.Chanin and A. Hauchecorne, *J. Geophys. Res.*, **96**, 5169 (1991).
5. C. D. Rodgers, *J. Atmos. Sci.*, **33**, 710 (1976); E. J. Fetzer and J. C. Gille, *J. Atmos. Sci.*, **51**, 2461 (1994).
6. J. W. Waters, *Atmospheric Remote Sensing by Microwave Radiometry*, M.A. Janssen, Ed. (Wiley, New York, 1993), chap.8; F. T. Bai ath et al., *J. Geophys. Res.* **98**, 10,751-10,762, 1993; J. W. Waters et al., *Nature*, **362**, 597 (1 993); L. Froidevaux et al., *J. Atmos. Sci.*, **51**, 2846 (1994); G. L. Manney et al., *Nature*, **370**, 429 (1994); M.L. Santee et al., *Science*, **267**, 849 (1995).
7. E. F. Fishbein et al., submitted to *J. Geophys. Res.*, (1995).
8. C. O. Hines, *Can. J. Phys.*, **38**, 1441 (1960).
9. G. L. Manney, R. W. Zurek, M. E. Gelman, A. J. Miller and R. Nagatani, *Geophys. Res. Lett.*, **21**, 2405 (1994).
10. M. R. Schoeberl and D. F. Strobel, *Dynamics of the Middle Atmosphere*, J.R. Holton and T. Matsuno, Eds. (Terra, Tokyo, 1984), pp.45-64.
11. S. Miyahara, Y. Hayashi and J. D. Mahlman, *J. Atmos. Sci.*, **43**, 1844 (1987).
- 12.1. Hirota and T. Niki, *J. Meteor. Soc. Japan*, **63**, 1055 (1985).
13. D.C. Fritts, *Rev. Geophys.*, **22**, 275 (1984).

14. E. L. Fleming, S. Chandra, J. J. Barnett, and M. Corney, *Adv. Space Res.*, **10**, **11** (1990).

14. T. Leblanc et al., *Geophys. Res. Lett.*, **22**, 1485 (1995).

16. We thank our MLS colleagues, especially G. L. Manney for providing wind data, W. G. Read for calculating weighting functions, and L. Froidevaux, L. S. Elson, R. F. Jarnot, D. A. Flower, E. F. Fishbein and R. R. Lay for helpful discussions. This work was performed at the Jet Propulsion Laboratory, California Institute of Technology, under contract with the National Aeronautics and Space Administration, and sponsored by NASA through the Upper Atmosphere Research Satellite Project.

Figure Captions

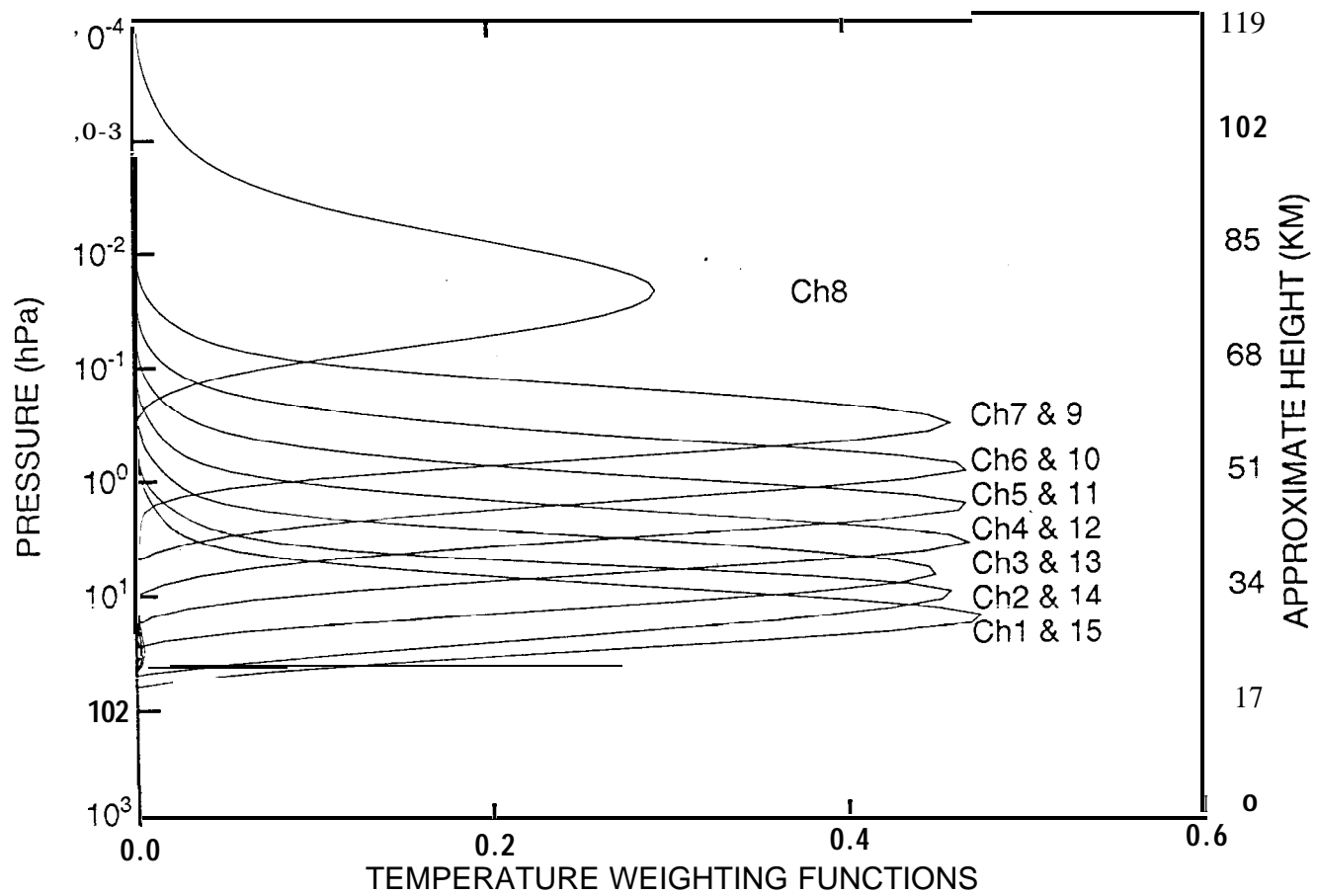
Figure 1. Temperature weighting functions of channels 1-15 when the MLS 63GHz radiometer views the limb at 18km (calculated by W. G. Read).

Figure 2. Maps of gravity wave variances observed during (a) “January” and (b) “July”. The variances are normalized by the squared mean radiance brightness temperature and colored in a logarithmic scale, i.e., $\log_{10}(\sigma_{GW}^2 / T^2)$. Winds (up to ~ 1 hPa) are derived from the US National Meteorological Center data [9] and averaged over the same periods.

Figure 3. Variance growth at different latitudes during “January” and “July” compared with the exponential growth expected for non-breaking gravity waves.

Figure 4. Zonal mean normalized IGW variances for “January” (top) and “July” (bottom). Contours are in units of 10^{-7} .

Figure



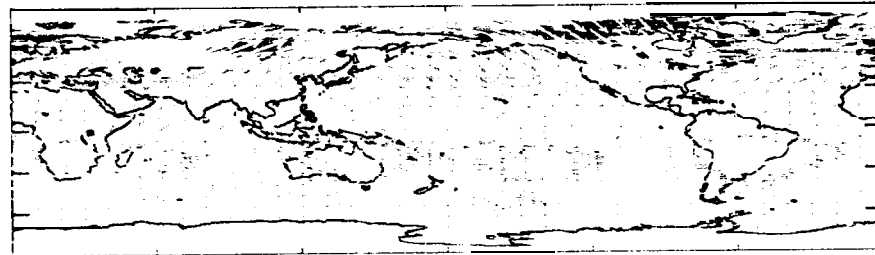
Ch. 8
(~80KM)



Ch. 7 & 9
(~61KM)



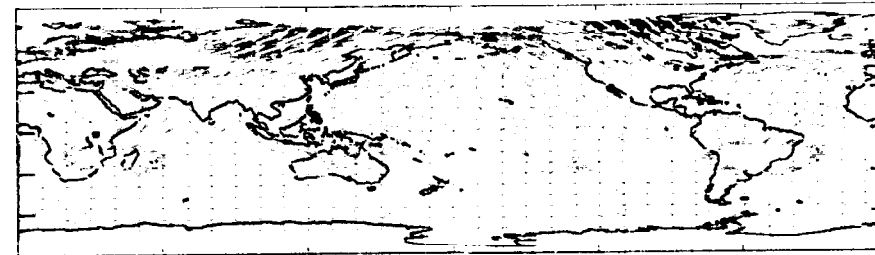
Ch. 6 & 10
(~53KM)



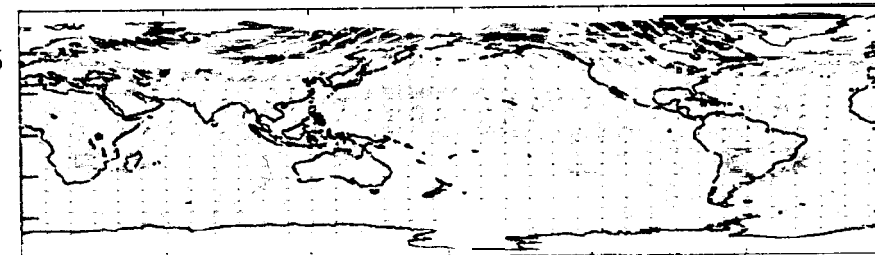
Ch. 5 & 11
(~48KM)



Ch. 4 & 12
(~43KM)



Ch. 3 & 13
(~38KM)

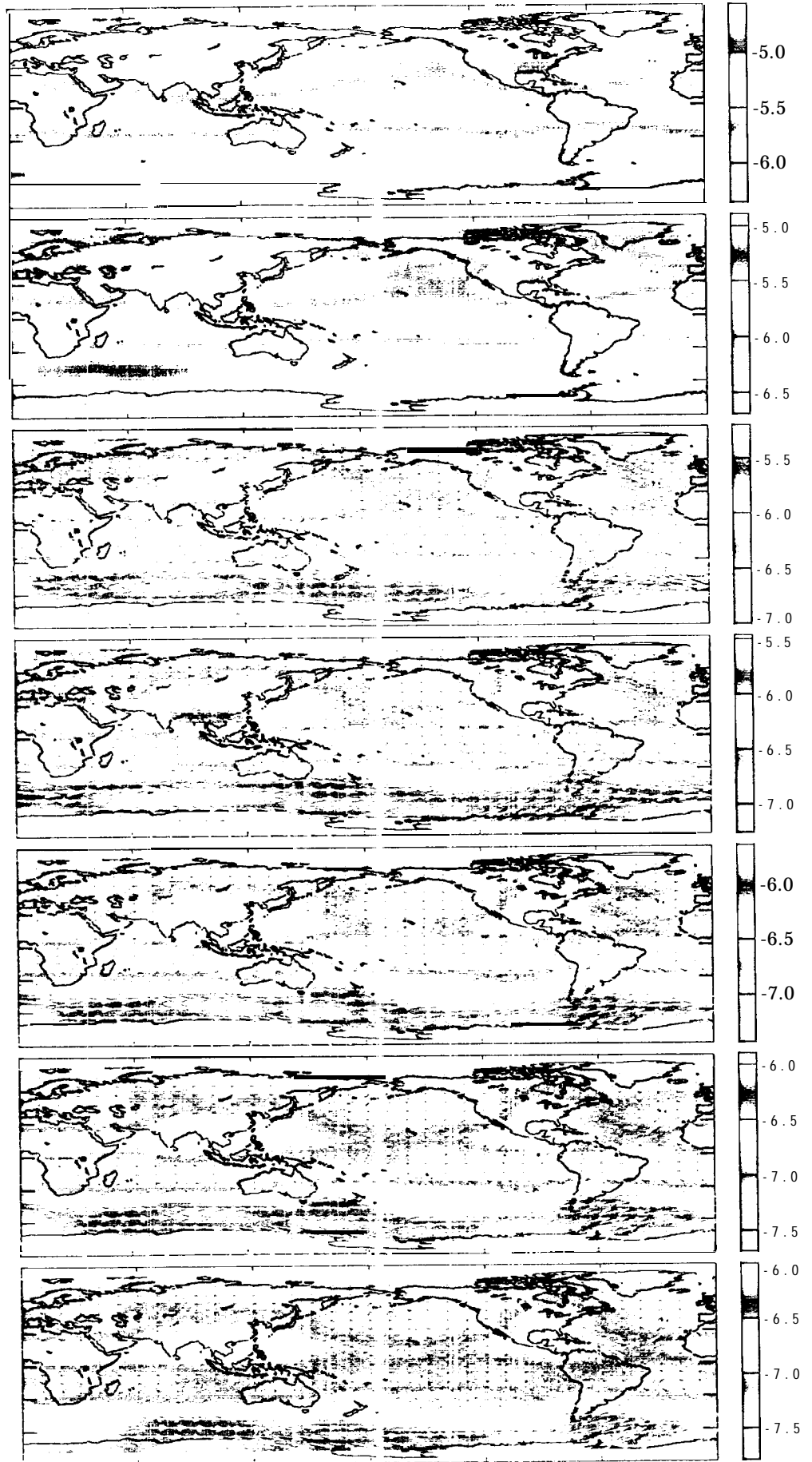


Ch. 2 & 14
(~33KM)



→
100 ins-l

(a)



(b)

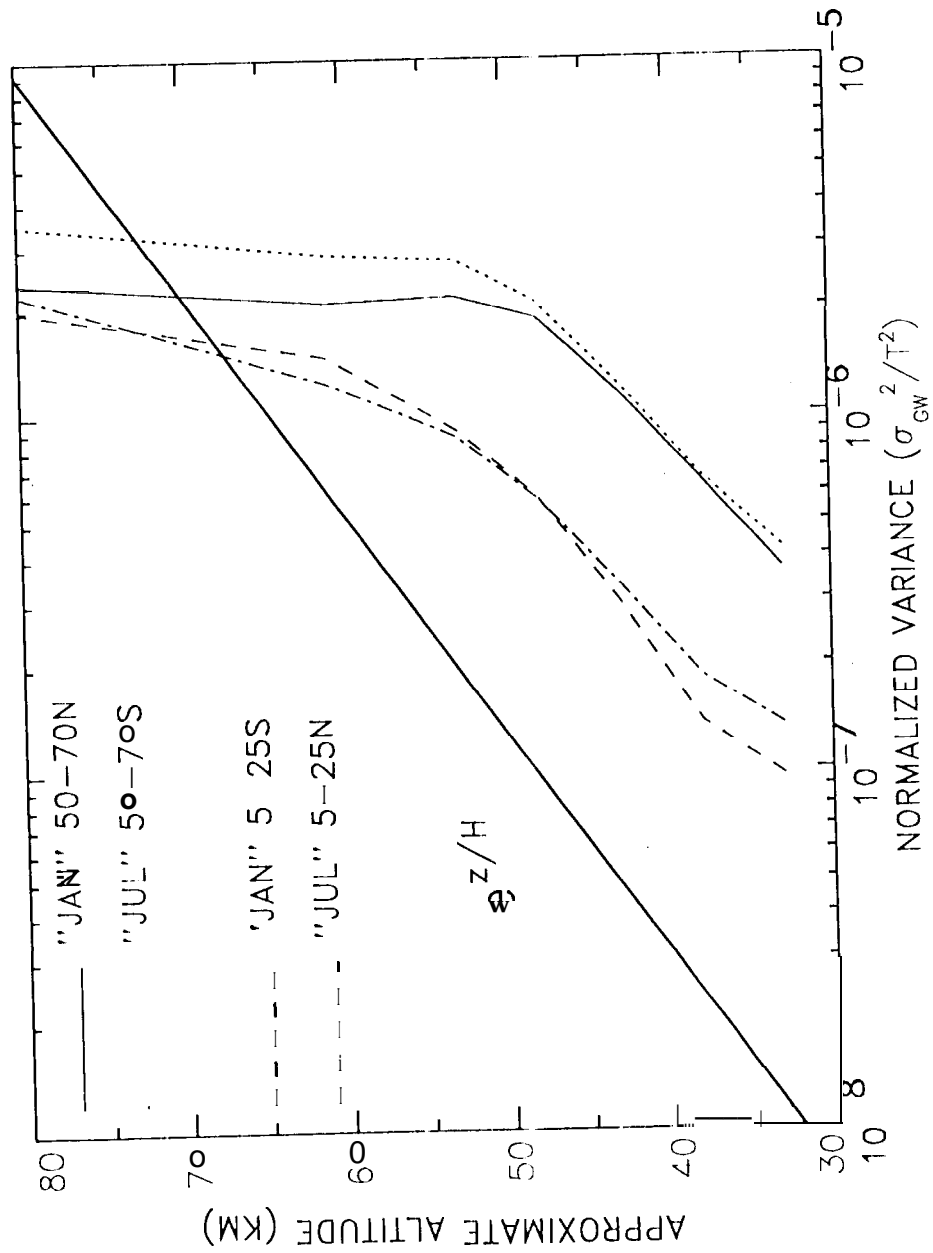


Figure 3

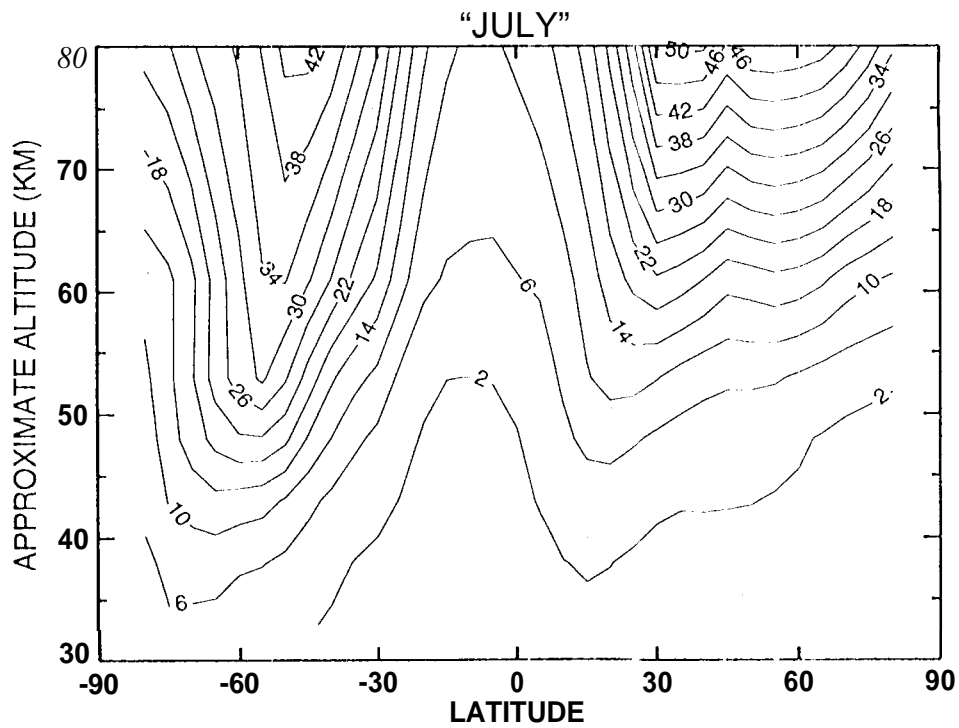
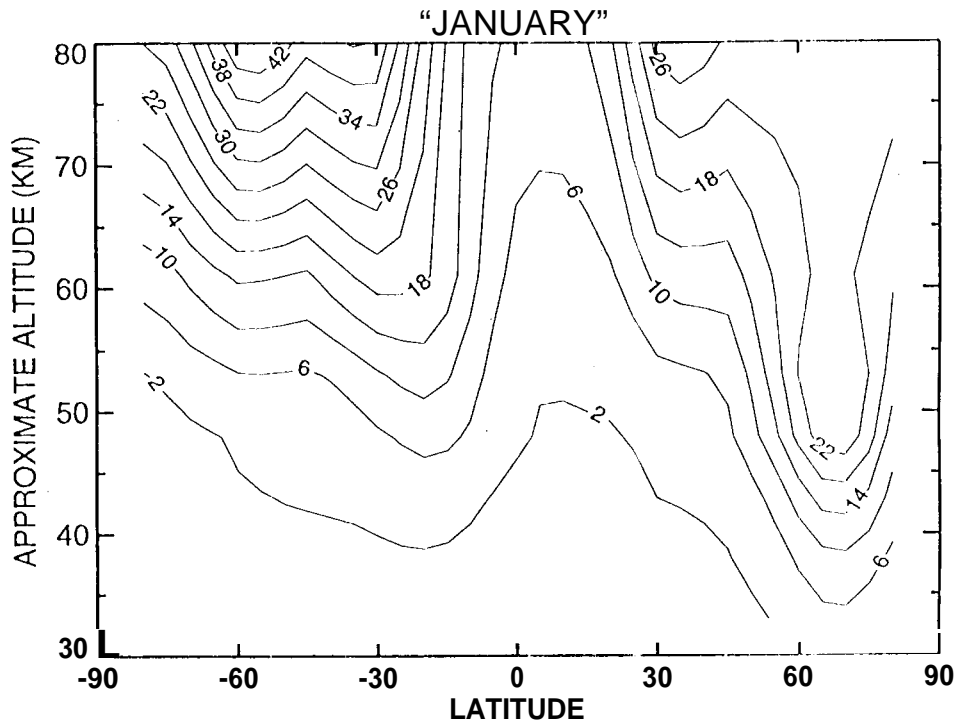


Figure 4